16th World Conference on Earthquake, 16WCEE 2017

Santiago Chile, January 9th to 13th 2017

Paper N° 4433

Registration Code: S-J1461792459

THE UCSB METHOD FOR SIMULATING BROADBAND GROUND MOTION USING CORRELATED RUPTURE PARAMETERS ON A FINITE FAULT

R. J. Archuleta[(1)], J. G. F. Crempien [(2)]

[(1)] *Professor Emeritus, University of California, Santa Barbara, ralph.archuleta@ucsb.edu.*
[(2)] *Research Scientist, Universidad de Chile and University of California, Santa Barbara, crempien@gmail.com.*

Abstract

The UCSB method produces broadband ground motion (0-25 Hz) for earthquakes with magnitudes between 5 and 8. For each earthquake scenario we generate kinematic rupture scenarios (50 stochastic realizations or more) that are characterized by Kostrov-like [1] slip-rate functions densely spaced on a finite fault area. The slip-rate functions are parameterized by the total slip, time to reach the maximum slip-rate (peak-time), the total time of slipping (rise-time), and time when slip starts (this determines the local rupture velocity). For each stochastic simulation each kinematic rupture parameter we filter white noise with a Von Karman power spectrum in the wavenumber domain to produce the spatial correlation. We use the correlations between each kinematic source parameter pair based on the dynamic rupture scenarios [2].

For each synthetic earthquake rupture scenario, we compute ground motion using the representation theorem. For this, we separate the wave propagation problem into a low- and high-frequency components separated at 1.0 Hz. The high-frequency Green's functions capture the geometrical decay with a simplified velocity structure. The high-frequency Green's functions will be later convolved with scattering functions. The high-frequency amplitude is modified using the detailed 1D velocity model for the velocity and density and the quarter-wavelength impedance [3]. The low-frequency ground motion is propagated from the source to the site using either a 1D or 3D velocity structure. We merge the low- and high-frequency ground motion by stitching these two in the wavelet domain [4]. Important to note is that the source is the same for both the low- and high-frequency components of ground motion.

So far we have successfully validated our method against well-recorded data produced by earthquakes in different tectonic regions such as California, Eastern United States, and Japan [5]. The metric for comparing the quality of the computed ground motion is acceleration response spectrum at distance up to 150 km from the fault. The comparisons look at the total bias between observed and computed response spectral ordinates at different periods as well as the dependence of the spectral ordinate on distance from the fault at various periods.

The UCSB method is an attractive solution to generate physics-based synthetic ground motion with minimal computational cost.

Keywords: keywords1, keywords2, (max. one line) Keywords should use Times New Roman 10 pt. font; Italic; separated by semicolon; Maximum 5

1. Introduction

Our main goal is to generate synthetic ground motion for engineering purposes such that the synthetics are as close as possible to observed ground motion from real earthquakes. We look to replicate the different seismic phase arrivals, e.g. the P-waves, S-waves, and surface waves. We also focus on matching as close as possible different engineering ground motion intensity parameters, such as peak ground acceleration (PGA) and response spectra at different oscillator frequencies. To achieve this goal, it is important to build a model that is sufficiently easy to use and capable of reproducing ground motion intensity measures of engineering interest, such as response spectra.

We propose a physics-based approach to estimate ground motion, in which we specify kinematic slip on a finite-fault to represent the spatiotemporal earthquake rupture process on a fault [4; 6]. Following [7], we use two sets of Green's functions that describe the low and high frequency content (typically separated at 1 Hz) in a hybrid manner, and convolve them with the *a priori* prescribed kinematic rupture process to compute low- and high-frequency ground motion. We stitch both low- and high-frequency ground motion in the wavelet domain [4].

We have made some modifications to the original method of [7], by using a slip-rate function that resembles a Kostrov shape [1]. It is tapered in time to assure a finite rise-time for the slip-rate function.

2. UCSB Method

2.1 Slip-Rate Function

After reviewing the dynamic rupture simulations of [2], we noticed that most of the slip-rate functions had a plateau between the peak-time and the rise-time, after which a rapid decay to zero slip-rate followed. With these observations, we decided to develop a new parameterization of the slip-rate function, inspired by the Kostrov [1] solution. Our approximation to a tapered Kostrov slip rate function is given in Eq. (1).

$$\dot{s}(t) = \begin{cases} \frac{At}{T_p}\sqrt{1+\frac{100}{T_p^2}}\sin\left(\frac{0.5\pi t}{T_p}\right), & 0 \le t < T_p \\ A\sqrt{1+\frac{100}{t^2}}, & T_p \le t < 0.7T_r \\ A\sqrt{1+\frac{100}{t^2}}\sin\left(\frac{0.5\pi(T_r-t)}{0.3T_r}\right), & 0.7T_t \le t < T_r \end{cases} \quad (1)$$

where t is time, A is a normalization constant, such that the total amount of slip is 1, T_p is the peak-time, and T_r is the rise-time. In Fig.1 we show different proposed slip-rate functions [8, 9, 4, 2], and the proposed slip-rate function (solid black line).

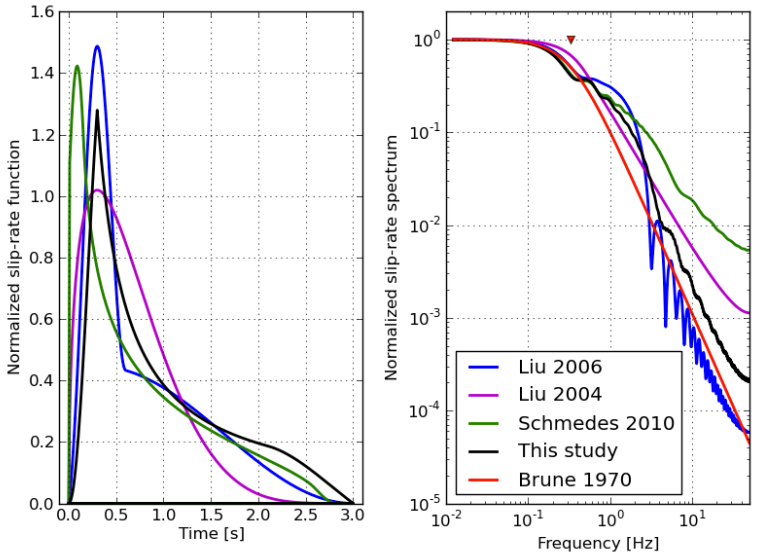

Fig. 1 – (a) We show an the slip-rate functions (normalized to unit slip) for a rise-time of 3 s and a peak-time of 0.3 s, of [4, 2, 9], and the function inspired by the solution of Kostrov [1] in blue, green, magenta and black solid lines respectively. (b) We show the slip-rate spectra of all parameterizations compared to a ω^{-2} spectrum (red solid line).

The proposed slip-rate function has a flat spectrum up to a corner frequency, after which, the spectrum has a ω^{-2} decay in displacement.

2.1 Probability Density Functions for Kinematic Rupture Parameters

For each kinematic rupture parameter, we draw a statistical realization based on different probability density functions (PDF). In Table 1 we list the different rupture parameters and their PDF functions.

Table 1 – Probability density functions used for the different kinematic rupture parameters that describe the slip-rate function at each sub-fault.

Kinematic Parameter	Slip	Rise-Time	Peak-Time	Rupture Velocity
Probability Density Function	Truncated Cauchy	Beta	On average 30% of rise-time	Beta

We truncate total slip for each sub-fault such that the maximum amount of slip on the entire fault does not exceed the upper limit proposed by [10]. The rise-time is assumed to be a beta distribution as shown in Eq. (2).

$$p(\tau) = C(\tau - \tau_{min})(\tau_{max} - \tau)^2 \quad (2)$$

where τ_{max} is chosen from the best fitting Brune's ω^{-2} model with prescribed target corner frequency f_c, and $\tau_{max} = 5\tau_{min}$. The peak-time is assumed to be 30% on average of the rise-time. The ratio of peak time to rise time is assumed to be uniformly distributed between 0.25 and 0.35. Finally, the rupture velocity is assumed to be a beta distribution such that the minimum value and the maximum value correspond to 0.7 and 0.9 of the average shear wave velocity.

2.3 Spatial Correlation of Source Parameters

To generate the distribution of slip on the fault, we follow the procedure of [4]. We first draw a realization of a white noise process, where the probability distribution of slip on each point of the fault is a truncated Cauchy distribution [4, 6]. After this process we filter the two-dimensional white noise with a von Karman filter shown in Eq. (3).

$$F(k_x, k_y) = \frac{1}{1+((C_L k_x)^2+(C_W k_y)^2)} \tag{3}$$

Where the C_L and C_W are the correlation lengths along strike and dip. The wavenumber along strike and dip are k_x and k_y respectively, which are assume to be equal and are related to the target magnitude as shown in Eq. (3).

$$log_{10}(C_L) = log_{10}(C_W) = M_W - 2 \tag{4}$$

The expression of correlation length is of paramount importance to the total ground motion variability as shown by [11, 12].

2.4 Correlation Between Source Parameters

We use the same mean correlations between source rupture parameters as found by [2]; correlation matrix is shown in Fig.2.

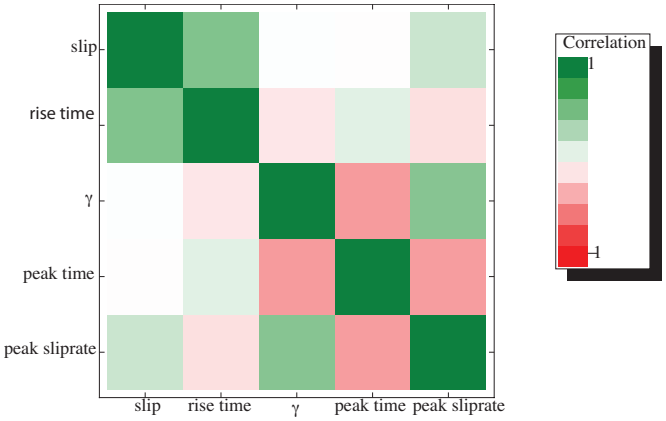

Fig. 2 – We show the correlation matrix between kinematic rupture parameters on the fault [8], where γ is the rupture velocity normalized to shear-wave velocity of the medium. This correlation is enforced in the UCSB method for computing ground motions from kinematic simulations of earthquakes.

The only correlations we do not enforce are those related to the peak-time. We have already assumed a uniform distribution for the ratio of peak-time to rise-time. After extensive tests we find that there is little difference between imposing a specific correlation to peak-time and rise-time versus assuming no particular correlation and setting peak-time to be a fraction of rise-time (on average).

2.5 Hybrid Wave Propagation with Green's Functions

One-dimensional velocity structures decrease the amplitude of ground frequencies higher than ~5 Hz [13] due to the low transmission coefficient SH to SH and SV to SV when the incidence angle is very high. High incidence angles are produced at distances far from the source. It is the principal physical mechanism of reduced amplitudes of higher frequencies far from the source. To solve this problem we have separated the wave propagation problem into two parts—a low and high frequencies separated at 1.0 Hz. For the low frequencies (LF) we keep regional

velocity structures that capture the arrival times of each seismic phase. For frequencies greater thna 1 Hz (HF) we use a layer over a half-space velocity structure, where the boundary between both media represents the Moho boundary. Since the HF model propagates waves faster than the regional velocity structure, we correct and shift the timing of the S-wave direct arrivals so that they agree with the regional velocity structure. Once we have computed Green's functions for both velocity structures, we use the representation theorem to produce synthetic ground motion for the same source model. We then stitch the two ground motion synthetics computed at each station in the wavelet domain [4]. In Fig.3 we show a synthetic simulation for LF and HF ground motion, as well as the broadband ground motion that formed by stitching the two motions in the wavelet domain. In Fig.3 we show the Fourier amplitude spectra (FAS) of acceleration for the LF, HF and broadband ground motion. This plot shows how the broadband follows closely the amplitude of the LF FAS at frequencies below 1 Hz;, after which the broadband FAS follows the HF ground motion.

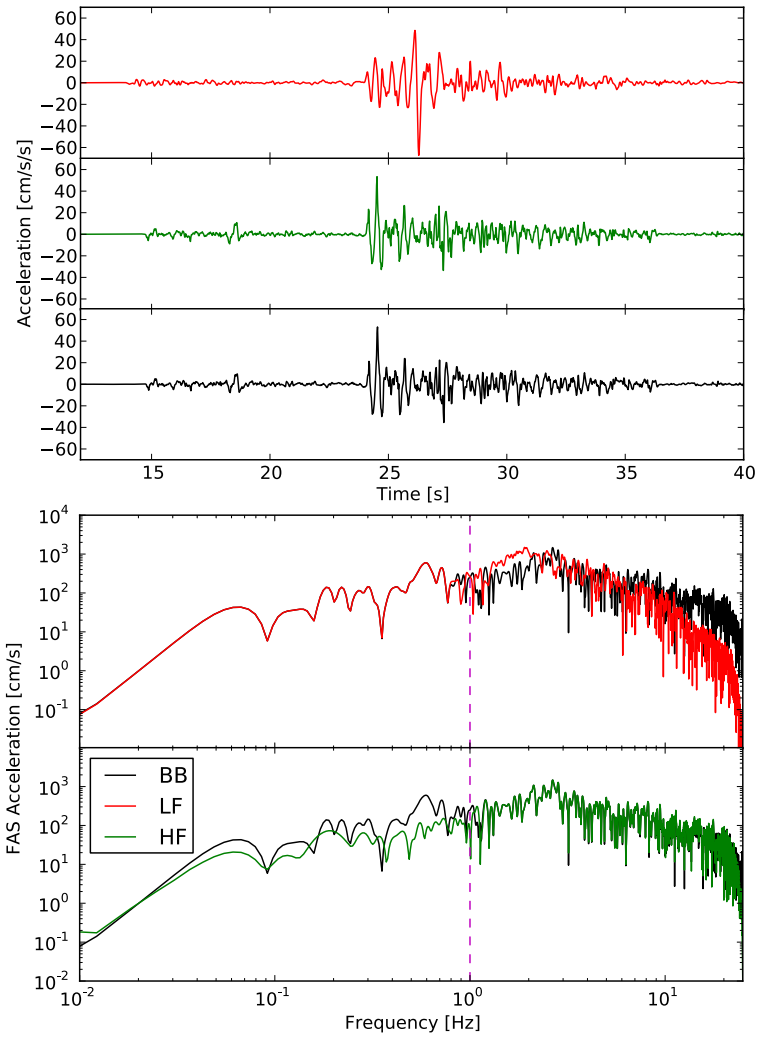

Fig. 3 – Combining low-frequency and high-frequency (depicted in red and green lines respectively) seismograms to form a broadband seismogram (in black line) at a distance of R_{rup}≈82 km from the source. For frequencies less than 1.0 Hz, the broadband FAS overlays almost identically the low-frequency FAS; from 1.0 Hz to 25 Hz, the broadband FAS is almost identical to the high-frequency FAS.

The difference in amplitude above 10 Hz between LF and HF can be approximamtely one order of magnitude lower, which means that regional synthetic Green's functions produce lower amplitude ground motion than recorded ground motion.

3. Validation Results

3.1 **M**6.73 1994 Northridge earthquake

We have done many simulations to check the proposed model against recorded ground motion from crustal earthquakes. The simulations are explained in detail in [5, 7]. We first show the results for the **M**6.73 1994 Northridge earthquake, which took place in Southern Califronia. For this earthquake we used a fault 20 km in length and 27 km in width; the hypocenter is located at ~19 km down dip and 16 km along strike. With this hypocenter location we make sure we can capture the directivity pulse that was created due to the advancing of the rupture front up dip. For each synthetic simulation of ground motion we computed response spectra, in particular RotD50. For each period we computed the bias as ln(data/model), where the data is the RotD50 acceleration spectrum for a particular station; and model is the acceleration spectrum (RotD50) determined from the synthetic ground motion. We performed 50 simulations for 39 stations. In Fig.4, we show the average bias for the 50 simulations at each of the 39 stations for eight spectral periods. The color represents the average bias of the 50 simulations at a particular period of the response spectrum.

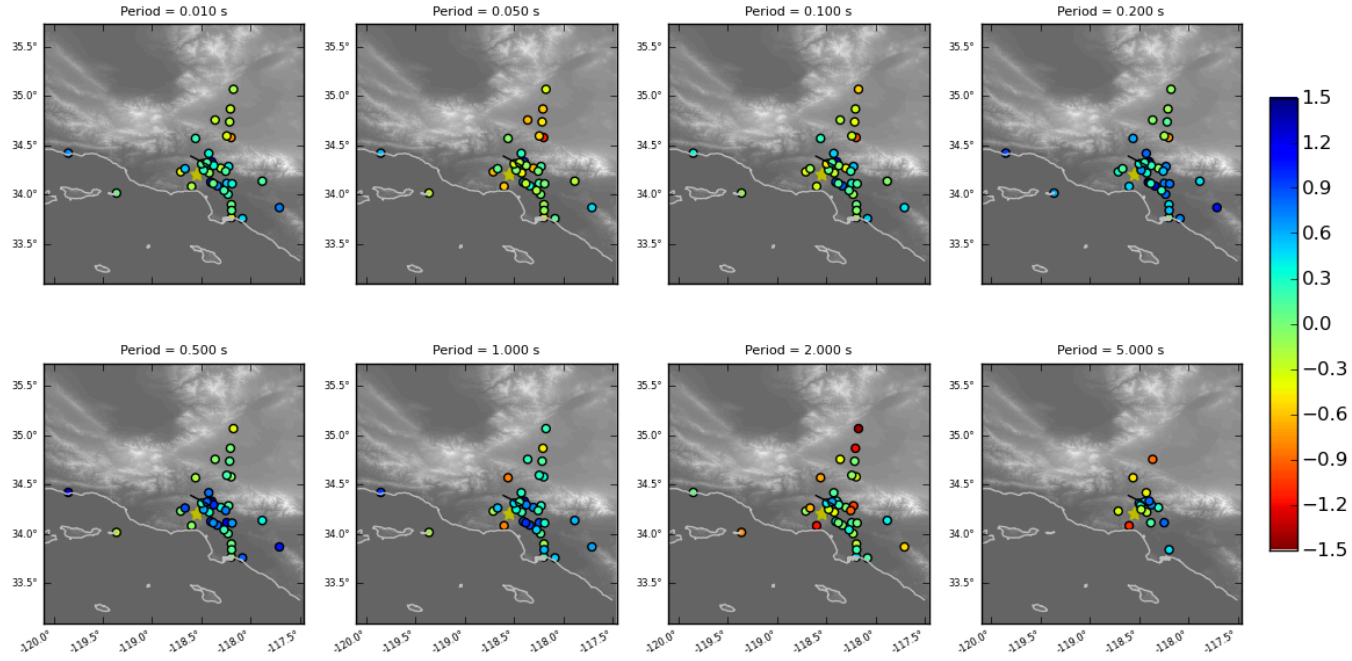

Fig. 4 – Map view of combined 50 realizations of bias at each station for the 1994 Northridge earthquake, for different period brackets. The upper segment of the fault is shown in black.

As the plots show, there is no particular spatial bias in the synthetic realizations of ground motion. To check the how the bias behaved with distance, we have plotted bias versus minimum distance to the fault (R_{rup}) in Fig.5.

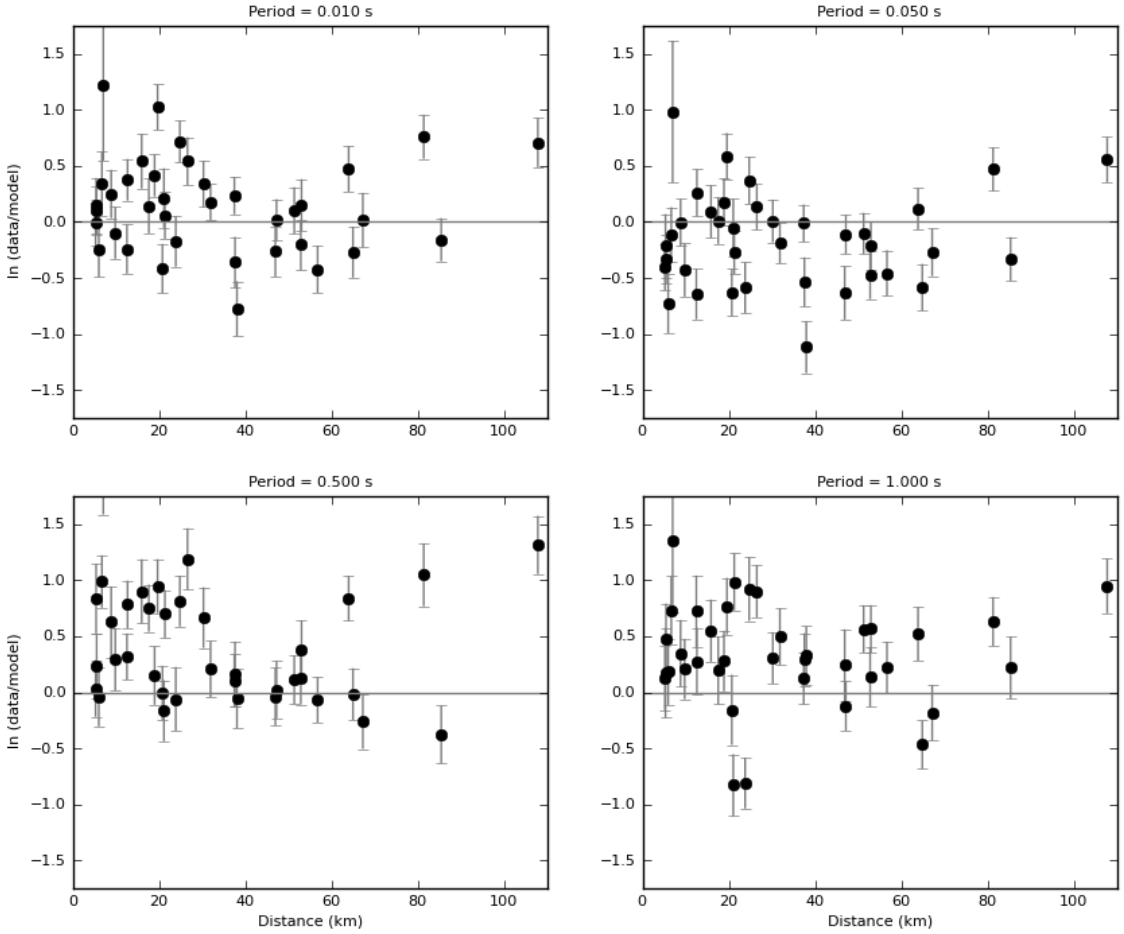

Fig. 5 – Each dot is the mean bias for 50 realizations at each station; distance is closest distance to the fault, and the whiskers show the bias extrema.

While we do not see any apparent bias of the UCSB model with distance, there is large scatter in the bias. We have also aggregated the biases for all stations and for all simulations into a single plot (Fig.6).

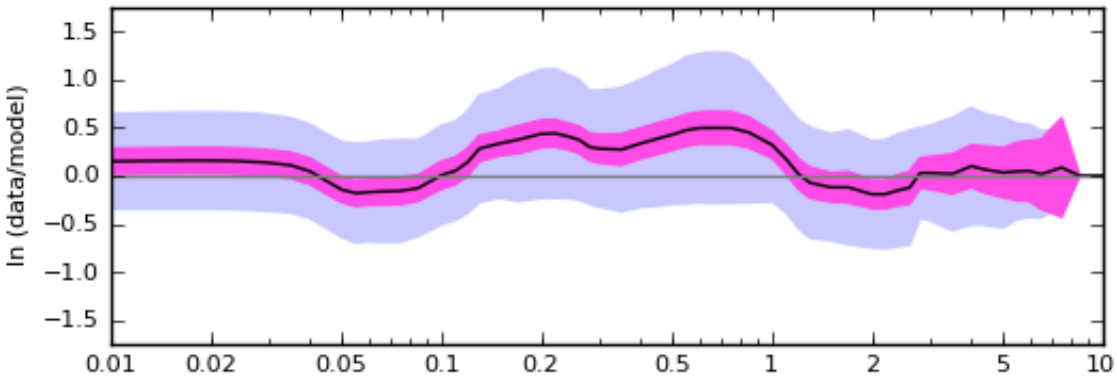

Fig. 6 – Combined 50 realizations of bias. The black line is the mean bias, the magenta corresponds to the 90% confidence interval of mean and the lavender region depicts the standard deviation around the mean.

We do not expect to have a zero bias over all periods because some of the simulated ground motions correspond to kinematic ruptures that may not resemble at all the real rupture process of the Northridge earthquake. Our main

goal with this particular validation is to have the true recorded observation within the range of our synthetic realizations.

3.2 **M**6.59 2000 Tottori earthquake

For the **M**6.59 2000 Tottori earthquake we have assumed a fault ~27 km length and 13.5 km wide. We have computed 50 simulations of a kinematic rupture on this fault and produced ground motion at the stations indicated by circles in Fig.7. The color of the stations represents the average bias of RotD50 spectral acceleration determined from the 50 rupture realizations. Each frame represents a different period of the response spectrum.

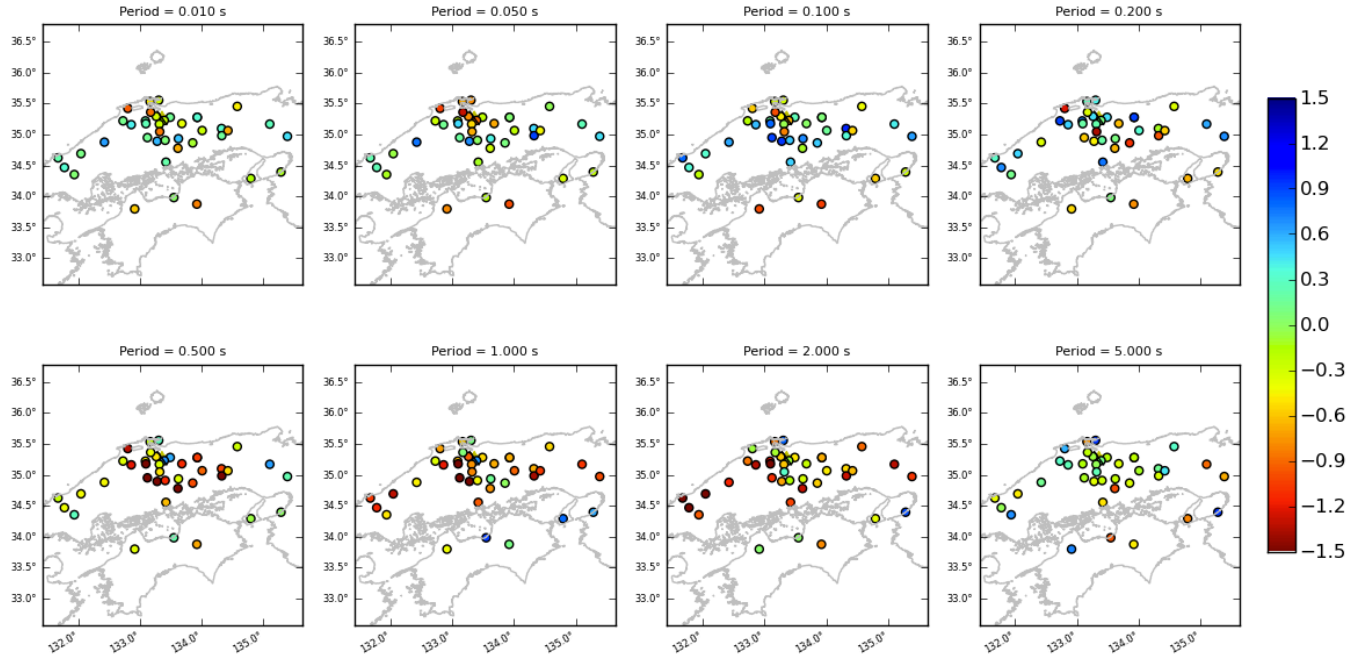

Fig. 7 – Map view of combined 50 realizations of bias at each station for the 2000 Tottori earthquake, for different period brackets. The upper segment of the fault is shown in black.

In Fig.8 we show the same results as a function of distance, for different periods of the response spectrum. The results show no bias with distance.

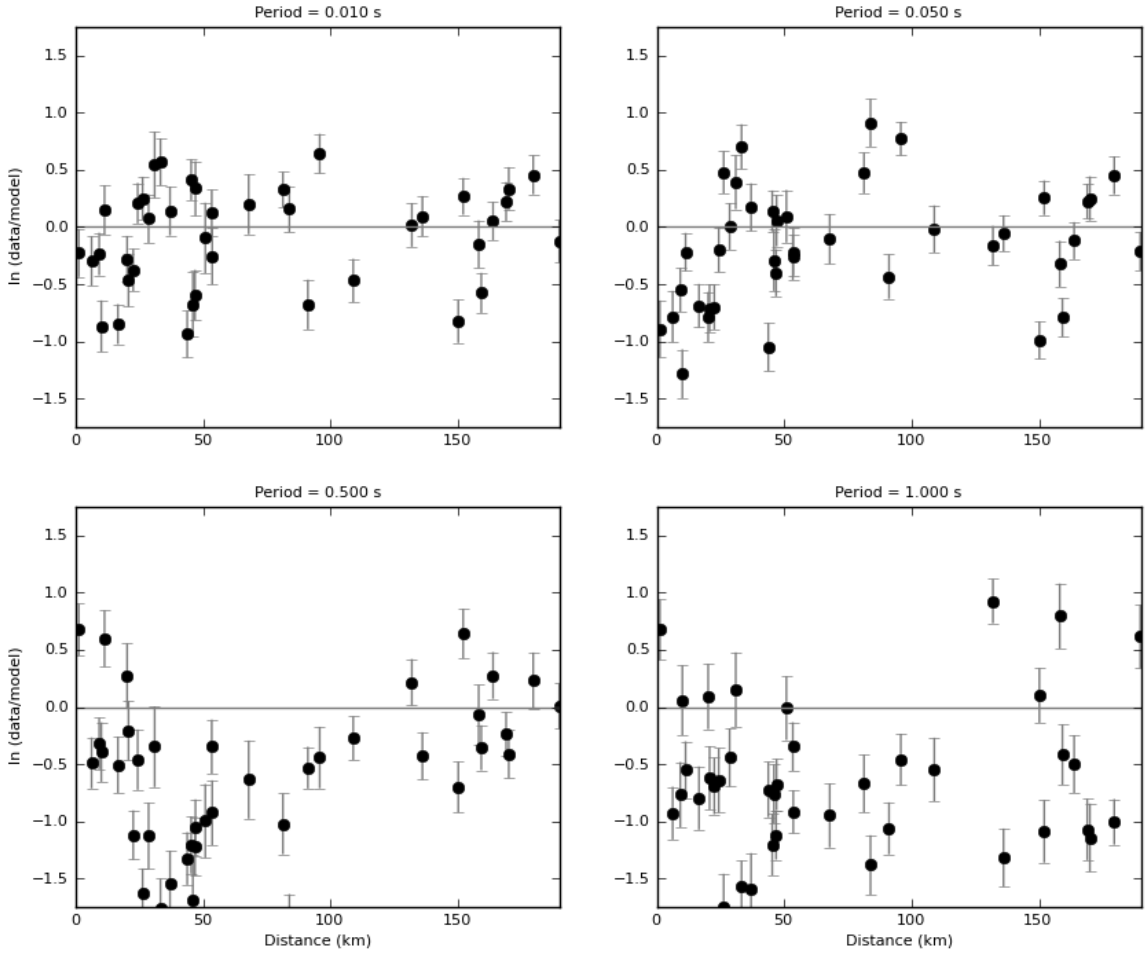

Fig. 8 – Each dot is the mean bias for 50 realizations at each station; distance is closest distance to the fault; the whiskers show the bias extrema.

In Fig.9 we show the combined average bias of all 50 realizations and all stations for the 2000 Tottori earthquake.

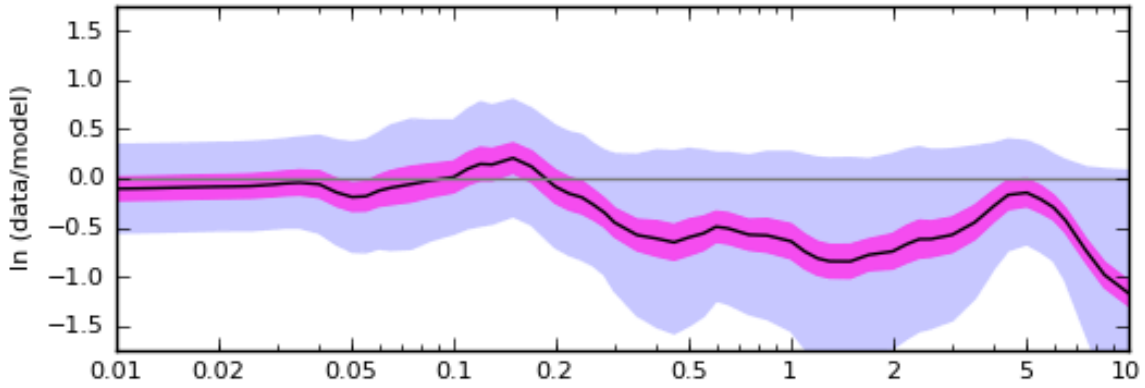

Fig. 9 – Combined 50 realizations of bias. The black line is the mean bias, the magenta corresponds to the 90% confidence interval of mean and the lavender region depicts the standard deviation around the mean.

The results show bias at the larger periods, which might be caused by the complex three-dimsional velocity structure in this region of Japan. This can likely be corrected in future synthetic simulations with 3D Green's functions.

3.1 **M**6.6 Reverse Earthquake Scenario GMPE

We have performed 50 rupture simulations for a **M** 6.6 earthquake on a vertical, strike-slip fault ~28 km in length and ~14 km in width. We compute the ground motion for 30 stations at the same closest distance (20 km) to the fault. The hypocenter is in one of 9 locations on the fault.. In Fig.10a we show the average bias of spectral acceleration at each station for all 50 rupture simulations. The average bias is close to zero at each station. In Fig.10b we compare the average (over all stations and all simulations) RotD50 response spectral values against an average RotD50 response spectrum based on the 2008 NGA West GMPE's. In Fig.10c show results for a **M** 6.6 reverse fault.

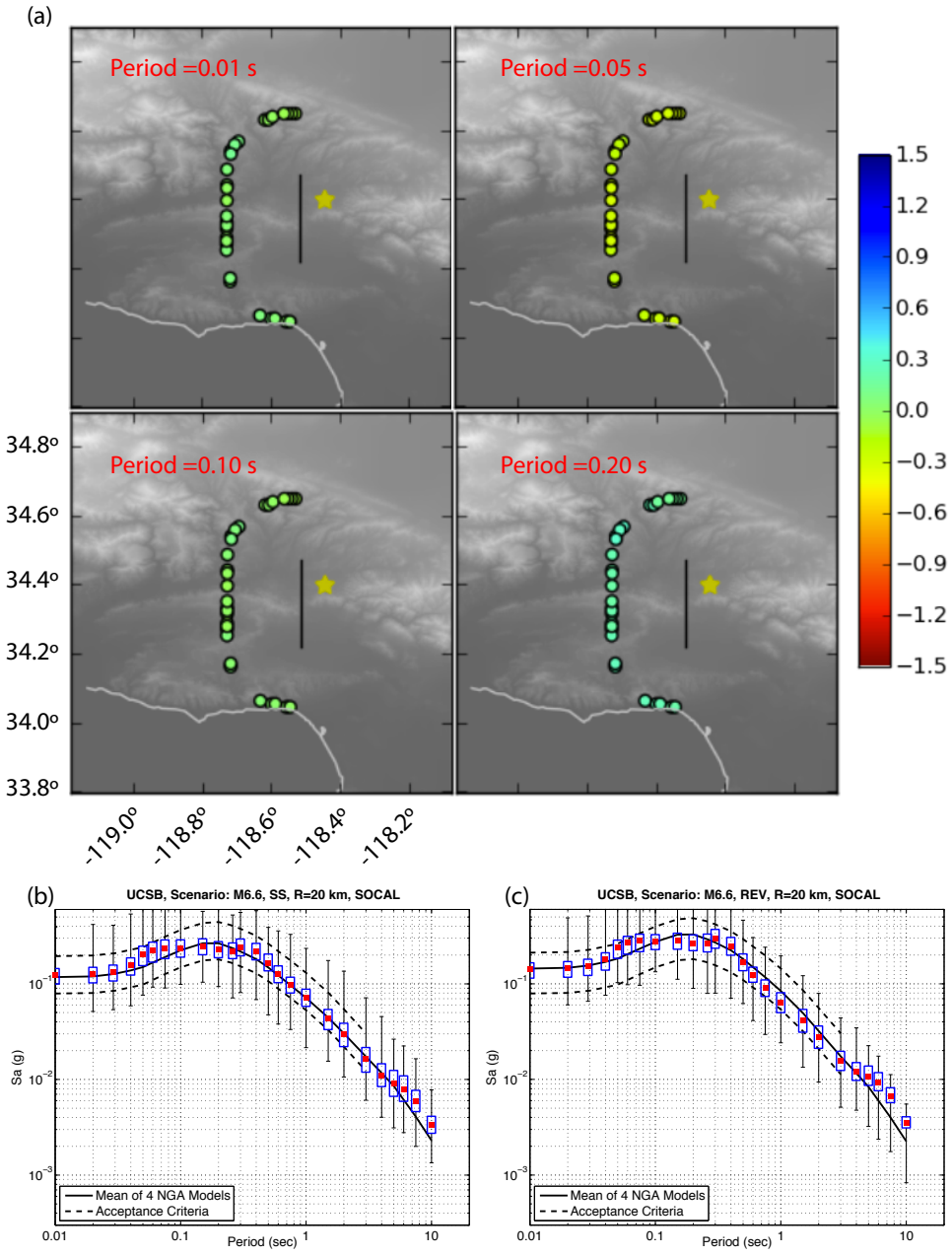

Fig. 10 – (a) shows the mean bias of 50 realizations of a **M** 6.6 strike-slip and reverse earthquake at each station. (b) The median RotD50 acceleration response spectral ordinate determined from all 50 simulations and 30 stations is shown as a red dot for **M** 6.6 strike-slip earthquake. The blue boxes represent 90% confidence intervals of mean and the black whiskers are the extrema of the 50 simulations and all stations. The black solid line is the average between the four 2008 NGA-West1 GMPE models, as described in Goulet *et al*. (2015). In all plots, results are for a set of stations at 20 km closest distance to the rupture plane.

The average of the simulations is close to the average GMPE's. This is the most important validation test, in our opinion, because the ground motion data was produced by several crustal earthquakes and recorded at several stations at different distances away from the fault.

3. Discussion

The UCSB method for ground motion simulation is an attractive approach with a sound physical basis. In the UCSB method the same source parameters determine both the low- and high-frequency ground motion. The source parameters are correlated with the correlations derived from dynamic rupture models. The spatial distribution of the parameters is determined from a 2D wavenumber spectrum with random phase allowing for asperities to be randomly assigned to areas of the fault. With the newly developed slip-rate function we have have found a the moment-rate spectrum that resembles a Brune ω^{-2} spectrum. This has improved the bias measured against the NGA West GMPE's.

The method is attractive because it does not require input parameters that are difficult to find in a specific tectonic region. Also, the method does not require a large number of parameters. It is easy to use, and can be applicable to many engineering projects that need broadband ground motion waveforms, e.g. determination of GMPE for regions with little or no recorded ground motion, nonlinear time-history analyses of structures for several plausible earthquake rupture scenarios, etc.

5. References

[1] Kostrov, B. V. (1964): Self-similar problems of propagation of shear cracks, *J. Appl. Math. Mech*, **30**, 1241-1248.

[2] Schmedes, J., R. J. Archuleta, and D. Lavallée (2010): Correlation of earthquake source parameters inferred from dynamic rupture simulations, *J. Geophys. Res.*, **115**, B03304, doi:10.1029/2009JB006689.

[3] Boore, D. M. and W. B. Joyner (1997): Site amplifications for generic rock sites, *Bull. Seismol. Soc. Am.* **87**, 327-341.

[4] Liu, P., R. J. Archuleta and S. H. Hartzell (2006): Prediction of broadband ground-motion time histories: Hybrid low/high-frequency method with correlated random source parameters, *Bull. Seismol. Soc. Am.,* **96**(6), 2118-2130, doi: 10.1785/0120060036.

[5] Goulet C., N. Abrahamson, P, Somerville, K. Woodell (2014): The SCEC broadband validation exercise for pseudo-spectral acceleration: Methodology for code validation in the context of seismic hazard analyses, *Seismol. Res. Lett.*, **86**, 1, 17-26, doi:10.1785/0220140104.

[6] Schmedes, J., R. J. Archuleta, and D. Lavallée (2013): A kinematic rupture model generator incorporating spatial interdependency of earthquake source parameters, *Geophys. J. Int.* **192** (3), 1116-1131. doi: 10.1093/gji/ggs02.

[7] Crempien, J. and R. J. Archuleta (2015): UCSB synthetic broadband ground motion method for kinematic simulations of earthquakes, *Seismol. Res. Lett.*, **86**, 1, 61-67, doi:10.1785/0220140103.

[8] Brune, J. N. (1970): Tectonic stress and spectra of seismic shear waves from earthquakes, *J. Geophys. Res.* **75**, 4997-5009. *Ibid*., Correction, 1971, **76**, 5002.

[9] Liu, P. and R. J. Archuleta (2004): A new nonlinear finite fault inversion with 3D Green's functions: Application to 1989 Loma Prieta, California, earthquake, *J. Geophys. Res.,* **109**, B02318, doi:10.1029/2003JB002625.

[10] McGarr, A. and J. B. Fletcher (2003): Maximum slip in earthquake fault zones, apparent stress, and stick-slip friction, *Bull. Seismol. Soc. Am.,* **93**(6) 2355–2362.

[11] Causse M., Cotton F., Mai P.M. (2010): Constraining the roughness degree of slip heterogeneity. *Journal of Geophysical Research: Solid Earth*, **115** (B5).

[12] Archuleta, R.J., and Crempien J.G.F. (2015): Ground motion variability from kinematic rupture scenarios. *Best Practices on Physics-based Fault Rupture Models for Seismic Hazard Assessment of Nuclear Installations*, Vienna, Austria.

[13] Crempien, J. G. F., and R. J. Archuleta (2014): Does a 1D velocity structure hurt or help ground motion predictions? *Seismol. Res. Lett.*, **85** (2), 508